A fatigue model for track-bed materials with consideration of the effect of coarse grain content

Yu Su, Yu Jun Cui, Jean Claude Dupla, Jean Canou, Shuai Qi

A fatigue model for track-bed materials with consideration of the effect of coarse grain content

Yu Su[1], Yu-Jun Cui[1], Jean-Claude Dupla[1], Jean Canou[1], Shuai Qi[1,2]

1: Laboratoire Navier/CERMES, Ecole des Ponts ParisTech (ENPC), 6 – 8 av. Blaise Pascal, Cité Descartes, Champs-sur-Marne, 77455 Marne – la – Vallée cedex 2, France

2: Dept. of Civil Engineering, Zhejiang University, 38 Zheda Road, Hangzhou 310027, China.

Corresponding author

Professor Yu-Jun Cui

Ecole des Ponts ParisTech, Laboratoire Navier/CERMES, 6 – 8 av. Blaise Pascal, Cité Descartes, Champs-sur-Marne, 77455 Marne – la – Vallée cedex 2, France

Tel.: +33 164153550

Fax: +33 164153562

E-mail address: yu-jun.cui@enpc.fr

Abstract

Previous studies showed that the permanent strain of interlayer soil in the French conventional railway substructure is highly dependent on the volumetric coarse grain content f_v (volumetric ratio of coarse grain to total sample). This study developed a fatigue model allowing the effects of coarse grain content f_v, stress state and number of loading cycles N on permanent strain to be accounted for. Data from the multi-stage loading cyclic tests of interlayer soil conducted at six different f_v values (0%, 5%, 10%, 20%, 35% and 45%) and five different maximum deviator stress Δq_{max} values (10 kPa, 15 kPa, 20 kPa, 25 kPa and 30 kPa) were reviewed and used for this purpose. The model parameters were determined by fitting the results from the tests at f_v = 0%, 5% and 35%. In order to validate the proposed fatigue model, the determined model parameters were then used to simulate the tests at f_v = 10%, 20% and 45%. The results obtained showed that the proposed model can well describe the permanent strain after a certain number of loading cycles, in the case of plastic shakedown.

Keywords: coarse grain content; permanent strain; fatigue model; cyclic triaxial tests; soil fabric

1 INTRODUCTION

Under the effect of long-term train circulation in the French conventional railway track, a new layer named interlayer was created, mainly by interpenetration of ballast and subgrade. Considering the high bearing capacity of the interlayer material corresponding to a mixture of ballast grains and fine soils, which was characterized by its high dry density of 2.4 Mg/m^3 (Trinh 2011), the French railway company (SNCF) decided to keep it as part of substructure in the national track renewal program. Field investigation showed that the proportion of ballast grains decreased over depth. Roughly, the interlayer could be divided into upper part which is dominated by ballast grains and lower part which is dominated by fine soils (Trinh et al. 2012). For the upper part, the effects of fine content and water contents on permanent strain were studied by Trinh et al. (2012), Cui et al. (2013), Duong et al. (2013, 2014, 2016) and Lamas-Lopez et al. (2014, 2016) by performing monotonic and cyclic triaxial tests. The results showed that the higher the water content, the larger the permanent strain. At saturated state, the higher the fine content, the larger the permanent strain. On the contrary, at unsaturated state, the higher the fine content, the lower the permanent strain due to the contribution of suction generated inside the fines. Wang et al. (2018a, 2018b, 2018c) further investigated the effect of volumetric coarse grain content f_v (volumetric ratio of coarse grain to total sample) on permanent strain using micro-ballast. A characteristic volumetric coarse grain content $f_{v\text{-}cha}$ was identified, below which the permanent strain decreased rapidly, and beyond which the permanent strain decreased relatively slowly. X-ray micro-tomography observation showed that the former case corresponded to a fine-matrix dominated structure, while the latter case corresponded to a coarse grain skeleton structure. Thus, it can be

60 deduced that the permanent deformation of interlayer soil increases over depth due to the
61 decreasing coarse grain content f_v. From a practical point of view, it is important to develop a
62 model, allowing the effect of f_v on permanent strain to be accounted for.

63 A few attempts have been made to describe the permanent strain with different factors
64 such as number of loading cycles *N*, stress state, soil physical state (water content and dry
65 density), etc. Based on experimental results, Barksdale (1972), Sweere (1990) and Hornych
66 (1993) developed various empirical approaches to describe the effect of *N* on permanent
67 strain, among which the model proposed by Hornych (1993) was validated by a large
68 number of tests and was adopted in French standard (AFNOR 1995). In general, these
69 models were developed based on cyclic tests subjected to a single-stage loading, which
70 required a large number of tests for the determination of parameters. To reduce the number
71 of tests and also the experimental dispersion related to samples variability, multi-stage
72 loading was generally recommended. Gidel et al. (2001) applied multi-stage loading on
73 unbound granular material, and found that the permanent strain increased significantly when
74 the deviator stress exceeded the past maximum value. Based on the results obtained, Gidel et
75 al. (2001) developed a model of permanent strain, accounting for both *N* and stress state. To
76 investigate the effect of water content on permanent strain of fouled ballast, Trinh et al.
77 (2012) performed multi-stage loading cyclic tests at various water contents. Based on the
78 results obtained, a fatigue model considering the effects of water content, *N* and stress state
79 was developed. More recently, Jing et al. (2018) proposed an approach to describe the
80 permanent strain of granular materials in low-traffic pavements, taking the effects of fine
81 content, water content, *N* and stress state into account. To the authors' knowledge, for the

82 interlayer soil of railway substructure, the effect of coarse grain content f_v on permanent
83 strain has not been taken into account.

84 This study aims at developing a model of permanent strain for interlayer soil,
85 accounting for the effects of number of loading cycles N, stress state and coarse grains
86 content f_v. Firstly, based on the multi-stage loading cyclic test results obtained by Wang et al.
87 (2018c), a general form of the model accounting for N, Δq_{max} and f_v was proposed. The
88 model parameters were determined based on a part of cyclic tests from Wang et al. (2018c).
89 In order to evaluate the performance of the proposed model, other tests were simulated using
90 the parameters determined previously. The advantage and limitation of the model were also
91 discussed.

92

93 **2 MODELLING OF PERMANENT STRAIN**

94 **2.1 Review of multi-stage loading cyclic tests**

95 Multi-stage loading cyclic tests were conducted on interlayer soil by Wang et al. (2018c). A
96 material simulating the interlayer soil was reconstituted by mixing fines with micro-ballast at
97 six different f_v values (0%, 5%, 10%, 20%, 35% and 45%). The samples were prepared by
98 dynamic compaction by keeping the fine soils inside the mixture at optimum water content
99 $w_{opt\text{-}f}$ = 13.7% and maximum dry density $\rho_{dmax\text{-}f}$ = 1.82 Mg/m^3, so that the suction developed
100 inside the fines was expected to be similar for all samples. The effect of coarse grain content
101 f_v on permanent strain was investigated through cyclic triaxial tests and the results are shown
102 in Fig. 1, with five different maximum deviator stress Δq_{max} values (10 kPa, 15 kPa, 20 kPa,
103 25 kPa and 30 kPa) and 90000 loading cycles for each Δq_{max}. It appears that the permanent

104 strain increased with the increasing loading cycles N and tended to stabilize at the end of
105 each loading stage for a given f_v value.

106 To visualize the soil fabric with different f_v values, X-ray μCT scans were performed
107 on as-compacted samples at six different f_v values (Fig. 2). It is observed that with the
108 increase of f_v from 0% to 10%, the soil fabric was dominated by the fine soils, with coarse
109 grains floating in it. At f_v = 20%, the contacts between aggregates started to develop, forming
110 local coarse grain skeletons by location. On the contrary, at f_v = 35% and 45%, the coarse
111 grains were in contact with each other, forming a global fabric of grain skeleton with fine
112 soils situated among grains. Thus, with the increase of f_v from 0% to 45%, the soil fabric
113 varies from a fine soils dominated structure to a coarse grain dominated structure.

114 **2.2 Development of a fatigue model**

115 Table 1 shows three widely applied fatigue models, with N by Hornych (1993), with N and
116 Δ?????? by Gidel et al. (2001), with N and Δ?????? and w by Trinh et al. (2012), allowing the
117 assessment of permanent strain produced under the effect of different variables. As this
118 study focuses on the modelling of the effect of f_v on permanent strain based on the cyclic test
119 results obtained by Wang et al. (2018c) under constant water content condition, the effect of
120 water content was not taken into account. Data from cyclic tests et different f_v values and at
121 various water content w values are needed to generalize the study to water content effect.
122 Most likely, the coupled effect of f_v w should be considered in that case. Table 1 shows that
123 the effects of N and other variables are separated to different terms (Gidel et al. 2001; Trinh
124 et al. 2012). Similarly, in this study, the proposed function k (??, Δ??????) is a term related
125 to the effects of f_v and Δq_{max}, while h (??) is a term related to N. The general form of this
126 model is established as follows:

$$\varepsilon_1^p(f_v, \Delta q_{max}, N) = k(f_v, \Delta q_{max}) \cdot h(N) \quad (1)$$

where ε_1^p is the permanent strain, $\Delta q_{\max}$ is the deviator stress level.

To develop the model, the first step is to determine the form of $h(N)$. Adopting the fatigue model $f(N)$ proposed by Hornych (1993) for this purpose (Eq. (2)):

$$f(N) = \varepsilon_1^{p*}(N) = \varepsilon_1^p(N) - \varepsilon_1^p(100) = A \cdot [1 - (\frac{N}{100})^{-B}] \quad \text{(for } N > 100 \text{ cycles)} \quad (2)$$

where ε_1^{p*} is the permanent strain after 100 cycles, parameter A represents the final stabilized maximum permanent strain, parameter B controls the evolution of permanent strain with increasing loading cycles N.

In order to consider the effect of $\Delta q_{\max}$, Eq. (2) is modified to Eq. (3). This modification is motivated by the change of physical meaning of parameter A while accounting for $\Delta q_{\max}$. As shown in Table 1, in the model of Hornych (1993), parameter A represents the stabilized maximum permanent strain. However, in the model considering N and $\Delta q_{\max}$ (Gidel et al. (2001), Trinh et al. (2012)), parameter a is used. The value of this parameter is close to '1' (a = 1.32 in Gidel et al. (2001); a = 0.76 in Trinh et al. (2012)) and it definitely does not represent the maximum permanent strain.

$$h(N) = a \cdot [1 - (\frac{N}{100})^{-B}] \quad \text{(for } N > 100 \text{ cycles)} \quad (3)$$

where B is a parameter.

After substituting Eq. (3) into Eq. (1), the fatigue model $\varepsilon_1^p(f_v, \Delta q_{max}, N)$ reads:

$$\varepsilon_1^p(f_v, \Delta q_{max}, N) = k(f_v, \Delta q_{max}) \cdot a \cdot [1 - (\frac{N}{100})^{-B}] \text{ (for } N > 100 \text{ cycles)} \quad (4)$$

Comparison between Eq. (4) and Eq. (2) shows that parameter 'A' in Eq. (2) corresponds to '$k(f_v, \Delta q_{max}) \cdot a$' in Eq. (4). Since parameter 'a' is close to unity, the physical meaning is the same for '$k(f_v, \Delta q_{max})$' and parameter 'A'. Different from 'A' representing the

maximum permanent strain (end-stage permanent strain), '$k(f_v, \Delta q_{max})$' represents the end-stage permanent strains at various loading levels Δ??????for each f_v..

Prior to determining the form of $k(f_v, \Delta q_{max})$in Eq. (4), the effects of coarse grain content f_v and deviator stress Δq_{max} on permanent strain need to be clarified. Fig. 3 shows the variations of end-stage permanent strain ε_1^p as a function of coarse grain content f_v for different Δq_{max} values. Note that the end-stage permanent strain ε_1^p was determined by a method proposed by Gidel et al. (2001), which was later applied by Lamas-Lopez (2016) and Wang et al. (2018c). The details of determination of that could be found in Wang et al. (2018c). It is worth noting that, based on the results obtained by this method, the value of end-stage permanent strain ε_1^p corresponds to that of maximum permanent strain at a given f_v and Δq_{max} values (Figure 3). It appears that a polynomial expression can be used to well describe their relationship. Fig.4 depicts the variations of the end-stage permanent strain ε_1^p with Δq_{max}. Interestingly, a linear relationship is identified for all f_v values. Thus, the expression of $k(f_v, \Delta q_{max})$ can be formulated as follows:

$$k(f_v, \Delta q_{max}) = \varepsilon_1^{p_0} \cdot [f_v^2 + b f_v + c] \cdot \left(\frac{\Delta q_{max}}{P_a} + d\right) \quad (5)$$

where $\varepsilon_1^{p_0}$, b, c, d are parameters, and P_a is atmospheric pressure, taken equal to 100 kPa.

In the model proposed by Trinh et al. (2012) (Table 1), a power relation was adopted to relate the end-stage permanent strain to Δq_{max} at various water contents as follows:

$$t(w, \Delta q_{max}) = \varepsilon_1^{p_0} \cdot (w + a_1) \cdot \left(\frac{\Delta q_{max}}{P_a}\right)^{\alpha} \quad (6)$$

where $\varepsilon_1^{p_0}$, a_1 and α are parameters, and $P_a = 100$ kPa.

A power relationship was obtained by Trinh et al. (2012) between the end-stage permanent strain ε_1^p and Δq_{max} for three different water contents w = 4%, 6% and 12%

171 (corresponding to S_r = 32%, 48% and 100%, respectively). In the case of constant water
172 content considered in this study ($w_{opt\text{-}f}$= 13.7%), a linear relationship is obtained with α = 1.
173 Further examination reveals that the linear relationship is also valid when the soil is
174 unsaturated (w = 4% and 6%) in the case of Trinh et al. (2012), as shown in Fig. 5.

175 After substituting Eq. (5) into Eq. (4), the fatigue model $\varepsilon_1^p(f_v, \Delta q_{max}, N)$ accounting
176 for the effect of coarse grain content f_v, maximum deviator stress Δq_{max} and the number of
177 loading cycles N is obtained:

178 $$\varepsilon_1^p(f_v, \Delta q_{max}, N) = \varepsilon_1^{p_0} \cdot [f_v^2 + bf_v + c] \cdot (\frac{\Delta q_{max}}{P_a} + d) \cdot \ a \cdot [1 - (\frac{N}{100})^{-B}]$$

179 (for N >100 cycles) (7)

180 where $\varepsilon_1^{p_0}$, b, c, d, a and B are parameters, and P_a=100 kPa.

181

182 **3 DETERMINATION OF MODEL PARAMETERS**

183 Wang et al. (2018c) investigated the effect of coarse grain content f_v on permanent strain
184 with six different f_v values (0%, 5%, 10%, 20%, 35% and 45%). The measured data from the
185 tests at f_v = 0%, 5%, 35% are used to determine the model parameters, with the following
186 two steps:

187 The first step is to determine four parameters $\varepsilon_1^{p_0}$, b, c and d by fitting Eq. (5) to the end-
188 stage permanent strains ε_1^p at f_v = 0%, 5%, 35%, as shown in Fig. 6. The values obtained
189 are $\varepsilon_1^{p_0}$= 2.40, b = -1.03, c = 0.45, d = -0.05.

190 The second step is to determine parameters a and B by fitting Eq. (7) to the measured
191 data at f_v = 0%, 5%, 35%. The parameters obtained are a = 1.20, B = 0.22.

192 Fig. 7 presents a comparison between the fitting curves and the measured data at f_v =
193 0%, 5%, 35%. It appears that the proposed fatigue model can well fit the experimental data.
194 Moreover, better fitting can be obtained when the permanent strain stabilizes at the ends of
195 loading stages.

196 After determining the model parameters, a sensitivity analysis of all parameters is
197 performed based on the results from the multi-stage loading cyclic test at f_v = 5% (Wang et
198 al. 2018c), and the results are shown in Fig. 8 and Fig. 9.

199 Since $k(f_v, \Delta q_{max})$ controls the end-stage permanent strain, the effects of
200 parameters $\varepsilon_1^{p_0}$, b, c and d on permanent strain curve are explained separately in Fig. 8. Fig.
201 8a shows that the increase of $\varepsilon_1^{p_0}$ leads to larger increase of end-stage permanent strain,
202 suggesting that parameter $\varepsilon_1^{p_0}$ controls the amplitude of permanent strain curve. The effect
203 of f_v on permanent strain is reflected through parameters b and c. It can be observed that with
204 the increase of parameter b, the amplitude of permanent strain curve changes slightly (Fig.
205 8b). In addition, Fig. 8c shows that the increase of parameter c gives rise to an increase of
206 permanent strain, suggesting that parameter c controls the effect of f_v through the amplitude
207 of permanent strain curve. Fig. 8d shows that the increase of parameter d results in parallel
208 movement of permanent strain curve, indicating that parameter d mainly controls the
209 interception of permanent strain curve.

210 Parameters a and B in h (N) expression affect the evolution of permanent strain with
211 loading cycles N. It can be observed in Fig. 9a that the larger the value of parameter B, the
212 larger the increase of permanent strain rate and the smaller the loading cycles N needed for
213 permanent strain stabilization. Therefore, parameter B governs the evolution of permanent

strain with increasing loading cycles *N,* which is consistent with previous studies (Hornych (1993); Gidel et al. (2001); Trinh et al. (2012); Jing et al. (2018)). In addition, parameter a affects the amplitude of permanent strain (Fig. 9b), with its value being around unity (i.e., a = 1.32 in Gidel et al. (2001); a = 0.76 in Trinh et al. (2012); a = 1.20 in the present study).

4 MODEL VALIDATION

In order to evaluate the performance of the proposed fatigue model, the data from the multi-stage loading cyclic tests at f_v = 10%, 20% and 45% are simulated. The model parameters determined previously based on the results at f_v = 0%, 5%, 35% are used for this purpose. Fig. 11 presents a comparison between the measured data and the corresponding simulated ones. It appears clearly that the parameters determined with f_v = 0%, 5% and 35% enable satisfactory simulations of the tests at f_v = 10%, 20% and 45%, with the coefficients of determination R^2 above 0.94 at various f_v values, as shown in Table 2.

5 DISCUSSION OF THE PROPOSED FATIGUE MODEL

5.1 The relation of f_v with parameters b and c

As shown in Eq. (5), the effect of f_v on the end-stage permanent strain is reflected through parameters b and c. Based on the determined parameters $\varepsilon_1^{p_0}$ and d, it can be observed from Fig. 10 that the end-stage permanent strain $\bar{\varepsilon}_1^p$ decreases with the increasing f_v at different Δq_{max} values. In order to investigate the relation of f_v with parameters b and c, the effect of Δq_{max} on the end-stage permanent strain ε_1^p is eliminated as follows:

$$\bar{\varepsilon}_1^p = \frac{k(f_v,\Delta q_{max})}{\varepsilon_1^{p_0}\cdot(\frac{\Delta q_{max}}{P_a}+d)} = f_v^2 + bf_v + c \quad (8)$$

The variation of $\bar{\varepsilon}_1^p$ with f_v follows a polynomial relationship. When $f_v = 0$,

$$c = \bar{\varepsilon}_1^p \tag{9}$$

Thus, parameter c represents the end-stage permanent strain $\bar{\varepsilon}_1^p$ at $f_v = 0$.

The changing trend of $\bar{\varepsilon}_1^p$ with f_v can be determined from Eq. (8):

$$\frac{\partial \bar{\varepsilon}_1^p}{\partial f_v} = 2f_v + b \tag{10}$$

Eq. (10) indicates that when the change of permanent strain $\bar{\varepsilon}_1^p$ with f_v becomes zero; i.e. $\frac{\partial \bar{\varepsilon}_1^p}{\partial f_v} = 0$,

$$b = -2f_v \tag{11}$$

Considering that f_v can vary from 0 to 100%, parameter b ranges from 0 to -2.

Based on the aforementioned determined parameters b and c, Eq. (12) can be obtained by substituting these values into Eq. (8):

$$\bar{\varepsilon}_1^p = f_v^2 - 1.03f_v + 0.45 \tag{12}$$

It can be observed from Fig. 10 that the determined parameters allow a reasonable description of the variation of end-stage permanent strain $\bar{\varepsilon}_1^p$ with f_v at different Δq_{max} values. The main discrepancy appears at Δq_{max} = 10 kPa, which is consistent with the observation shown in Fig. 7 and Fig. 11.

5.2 Interpretation of permanent strain behaviors by shakedown theory

In terms of permanent strain behaviors, three categories are defined in shakedown theory (Werkmeister et al. 2001, 2004; Song et al. 2010): category A (plastic shakedown)

characterized by stabilized permanent strain with loading cycles N, category B (plastic creep) characterized by failure at a large N, and category C (incremental collapse) characterized by failure at a small N. The criterion to classify the three categories is dependent on the accumulated permanent strain. Following the French standard AFNOR (2004), the limit of category A is reached when $\varepsilon_{1\,5000}^{p} - \varepsilon_{1\,3000}^{p} > 0.45 \times 10^{-4}$, where $\varepsilon_{1\,5000}^{p}$ and $\varepsilon_{1\,3000}^{p}$ are accumulated permanent strains at N = 5000 and 3000, respectively. In all the tests conducted by Wang et al. (2018c), the maximum difference between $\varepsilon_{1\,5000}^{p}$ and $\varepsilon_{1\,3000}^{p}$ occurs at f_v = 0% and Δq_{max} = 30 kPa, equal to 0.3×10^{-4}, smaller than the plastic shakedown limit. Thus, the response of all tests considered is within category A. Fig. 11 shows that the proposed fatigue model is relevant to describe the permanent strain behavior for category A. This confirms the assumption made by Hornych (1993) in their model that the permanent strain reaches a finite limit as loading cycles N tends toward infinite.

6 CONCLUSIONS

In order to model the effect of f_v on permanent strain of interlayer soil, a fatigue model $\varepsilon_1^p(f_v, \Delta q_{max}, N)$ was developed based on the results from multi-stage loading cyclic tests conducted by Wang et al. (2018c), at six different f_v values (0%, 5%, 10%, 20%, 35% and 45%) and five different Δq_{max} values (10 kPa, 15 kPa, 20 kPa, 25 kPa and 30 kPa), with 90000 loading cycles for each Δq_{max}. The proposed fatigue model accounts for the effects of coarse grain content f_v, maximum deviator stress Δq_{max} and loading cycles N on permanent strain. The model parameters were determined by fitting the cyclic tests at f_v = 0%, 5% and 35%, and then used to simulate the tests at f_v = 10%, 20% and 45%. A good agreement was

obtained between the measurements and simulations, showing the performance of the proposed fatigue model for predicting permanent strain.

It is worth noting that the proposed model is valid when the permanent strain stabilizes at a certain number of cycles *N*. In other words, it can only describe the permanent strain of category A (plastic shakedown). Moreover, the fatigue model $\varepsilon_1^p(f_v, \Delta q_{max}, N)$ has not taken the effect of water content into account. Further experimental data are needed to take this effect into consideration.

ACKNOWLEDGEMENTS

This work was supported by the Chinese Scholar Council (CSC) and Ecole des Ponts ParisTech.

NOTATIONS

ε_1^p	permanent strain
$\varepsilon_1^{p*}(N)$	permanent strain from 100 cycles to *N* cycles
f_v	volumetric coarse grain content
N	number of loading cycles
Δp_{max}	maximum mean stress
Δq_{max}	maximum deviator stress
S_r	degree of saturation
w	water content
$w_{opt\text{-}f}$	optimum water content of fine soils
$\rho_{dmax\text{-}f}$	maximum dry density of fine soils

289

290 REFERENCES

291 AFNOR, 1995. NF P98-235-1—Test relating to pavements. Unbound granular materials.
292 Part 1: Repeated Loading Triaxial Test.

293 AFNOR, 2004, NF EN 13286-7—Unbound and Hydraulically Bound Mixtures. Part 7:
294 Cyclic Load Triaxial Test for Unbound Mixtures.

295 Barksdale RD. Laboratory evaluation of rutting in base course materials. In Presented at the
296 Third International Conference on the Structural Design of Asphalt Pavements,
297 Grosvenor House, Park Lane, London, England, Sept. 11-15, 1972. 1972 Sep (Vol. 1,
298 No. Proceeding).

299 Cui YJ, Duong TV, Tang AM, Dupla JC, Calon N, Robinet A. Investigation of the hydro-
300 mechanical behaviour of fouled ballast. Journal of Zhejiang University Science A. 2013;
301 14(4):244-55.

302 Duong TV, Tang AM, Cui YJ, Trinh VN, Dupla JC, Calon N, Canou J, Robinet A. Effects
303 of fines and water contents on the mechanical behavior of interlayer soil in ancient
304 railway sub-structure. Soils and foundations. 2013; 53(6):868-78.

305 Duong TV, Cui YJ, Tang AM, Dupla JC, Canou J, Calon N, Robinet A. Investigating the
306 mud pumping and interlayer creation phenomena in railway sub-structure. Engineering
307 geology. 2014; 171:45-58.

308 Duong TV, Cui YJ, Tang AM, Dupla JC, Canou J, Calon N, Robinet A. Effects of water
309 and fines contents on the resilient modulus of the interlayer soil of railway substructure.
310 Acta Geotechnica. 2016; 11(1):51-9.

311 Gidel G, Hornych P, Breysse D, Denis A. A new approach for investigating the permanent
312 deformation behaviour of unbound granular material using the repeated loading triaxial
313 apparatus. Bulletin des laboratoires des Ponts et Chaussées. 2001 July (233).
314 Hornych P. Étude des déformations permanentes sous chargements répétés de trois graves
315 non traitées. Bulletin de liaison des Laboratoires des Ponts et Chaussées. 1993 (184).
316 Jing P, Nowamooz H, Chazallon C. Permanent deformation behaviour of a granular material
317 used in low-traffic pavements. Road Materials and Pavement Design. 2018; 19(2):289-
318 314.
319 Lamas-Lopez F, d'Aguiar SC, Robinet A, Cui YJ, Calon N, Canou J, Dupla JC, Tang AM.
320 In-situ investigation of the behaviour of a French conventional railway platform.
321 InProceedings of the transportation research board 94th annual meeting. Washington,
322 DC 2014 Oct (pp. 15-1076).
323 Lamas-Lopez, Francisco. Field and laboratory investigation on the dynamic behaviour of
324 conventional railway track-bed materials in the context of traffic upgrade. PhD diss.,
325 Paris Est, 2016.
326 Sweere, G.T.H., Unbound Granular Bases for Roads. PhD Thesis. Delft, Netherlands, 1990.
327 Song Y, Ooi PS. Interpretation of shakedown limit from multistage permanent deformation
328 tests. Transportation Research Record. 2010 Jan; 2167(1):72-82.
329 Trinh VN. Comportement hydromécanique des matériaux constitutifs de plateformes
330 ferroviaires anciennes (PhD Thesis). Ecole Nationale des Ponts et Chaussées,
331 Université Paris-Est. 2011.

Trinh VN, Tang AM, Cui YJ, Dupla JC, Canou J, Calon N, Lambert L, Robinet A, Schoen O. Mechanical characterisation of the fouled ballast in ancient railway track substructure by large-scale triaxial tests. Soils and foundations. 2012; 52(3):511-23.

Werkmeister S, Dawson AR, Wellner F. Permanent deformation behavior of granular materials and the shakedown concept. Transportation Research Record. 2001; 1757(1):75-81.

Werkmeister S, Dawson AR, Wellner F. Pavement design model for unbound granular materials. Journal of Transportation Engineering. 2004; 130(5):665-74.

Wang HL, Chen RP, Qi S, Cheng W, Cui YJ. Long-term performance of pile-supported ballastless track-bed at various water levels. Journal of Geotechnical and Geoenvironmental Engineering. 2018a; 144(6):04018035.

Wang HL, Cui YJ, Lamas-Lopez F, Calon N, Saussine G, Dupla JC, Canou J, Aimedieu P, Chen RP. Investigation on the mechanical behavior of track-bed materials at various contents of coarse grains. Construction and Building Materials. 2018b; 164:228-37.

Wang HL, Cui YJ, Lamas-Lopez F, Dupla JC, Canou J, Calon N, Saussine G, Aimedieu P, Chen RP. Permanent deformation of track-bed materials at various inclusion contents under large number of loading cycles. Journal of Geotechnical and Geoenvironmental Engineering. 2018c; 144(8):04018044.

LIST OF TABLES

LIST OF FIGURES

Table 1. Fatigue models accounting for the effect of different factors on permanent strain reported in literatures

Reference	Variable	Fatigue model
Hornych (1993)	1) N	$\varepsilon_1^p = f(N) = A \cdot [1 - (\frac{N}{100})^{-B}])$
Gidel et al. (2001)	1) N 2) Δq_{max}	$\varepsilon_1^p = g(\Delta p_{max}, \Delta q_{max}) \cdot h(N)$ $= g(\Delta p_{max}, \Delta q_{max}) \cdot a \cdot \left[1 - \left(\frac{N}{100}\right)^{-B}\right]$ $g(\Delta p_{max}, \Delta q_{max}) = \varepsilon_1^{p_0} (\frac{l_{max}}{p_a})^n \frac{1}{(m + \frac{s}{\Delta p_{max}} - \frac{\Delta q_{max}}{\Delta p_{max}})}$
Trinh et al. (2012)	1) N 2) Δq_{max} 3) w	$\varepsilon_1^p = t(w, \Delta q_{max}) \cdot h(N)$ $= t(w, \Delta q_{max}) \cdot a \cdot [1 - (\frac{N}{100})^{-B}]$ $t(w, \Delta q_{max}) = \varepsilon_1^{p_0} * (w + a_1) * (\frac{\Delta q_{max}}{p_a})^{\alpha}$

Table 2. Coefficients of determination R^2 of cyclic test results at various f_v values

f_v	0%	5%	10%	20%	35%	45%
R^2	0.95	0.97	0.94	0.97	0.94	0.94

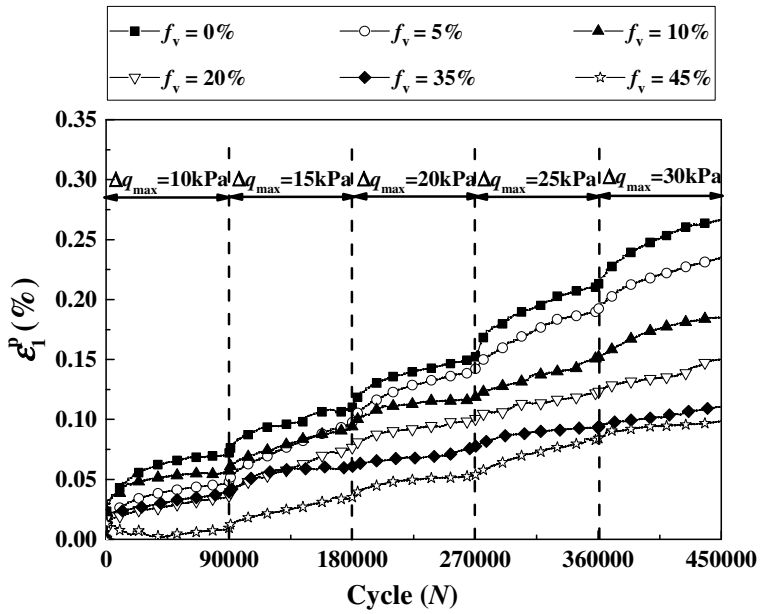

Fig. 1. Variations of permanent strain with the number of loading cycles N at different f_v and Δq_{max} values (after Wang et al. 2018c)

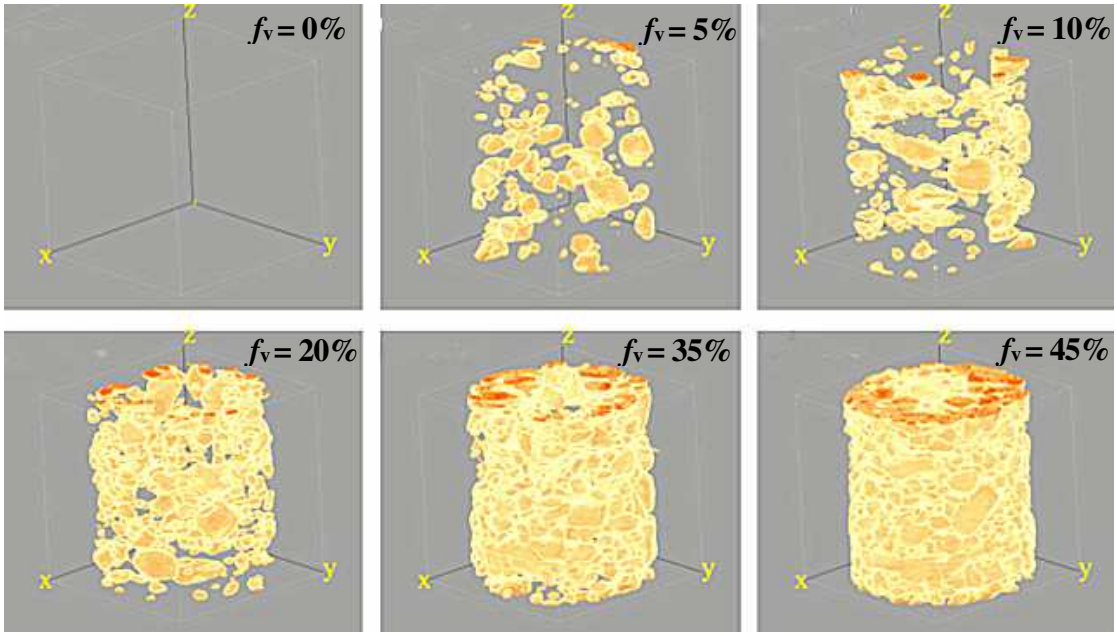

Fig. 2. 3D views of the coarse grain distributions in compacted samples (after Wang et al. 2018c)

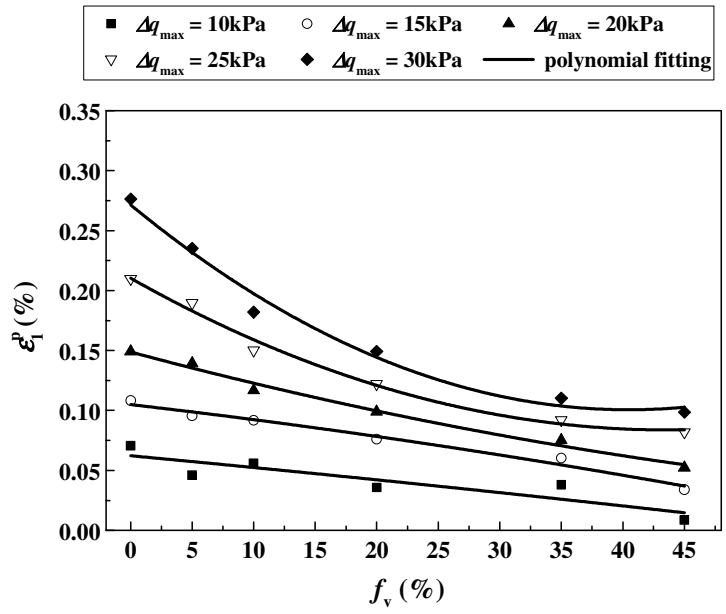

Fig. 3. Polynomial fitting of end-stage permanent strain ε_1^p with f_v at different Δq_{max} values (after Wang et al. 2018c)

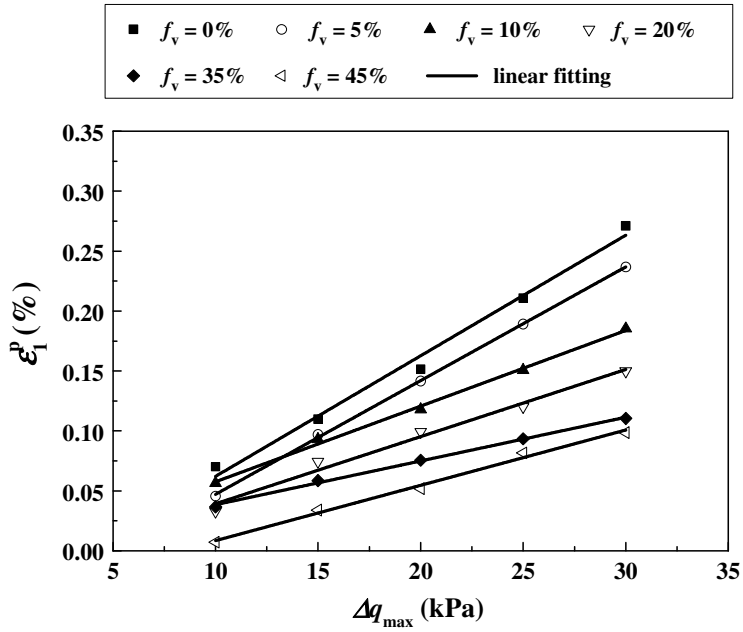

Fig. 4. Linear fitting of end-stage permanent strain ε_1^p with Δq_{max} at different f_v values

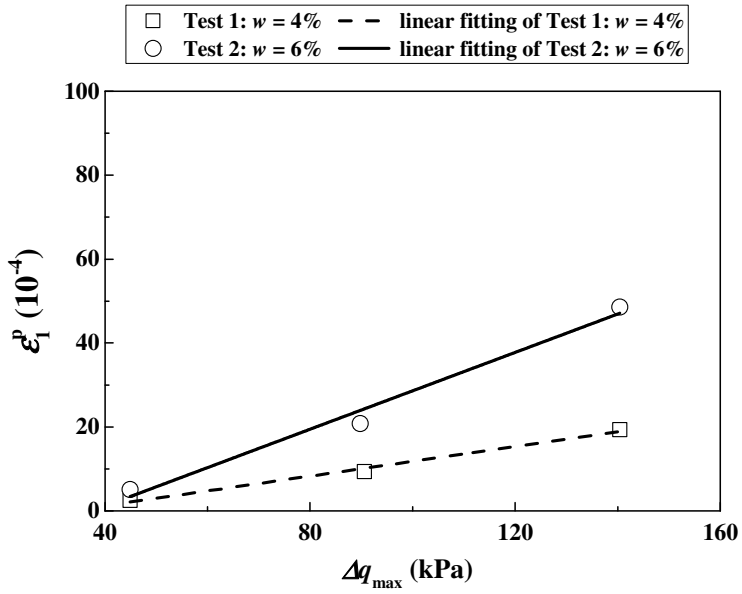

Fig. 5. Linear fitting of end-stage permanent strain ε_1^p with $\Delta q_{\max}$ at unsaturated water contents (after Trinh et al. 2012)

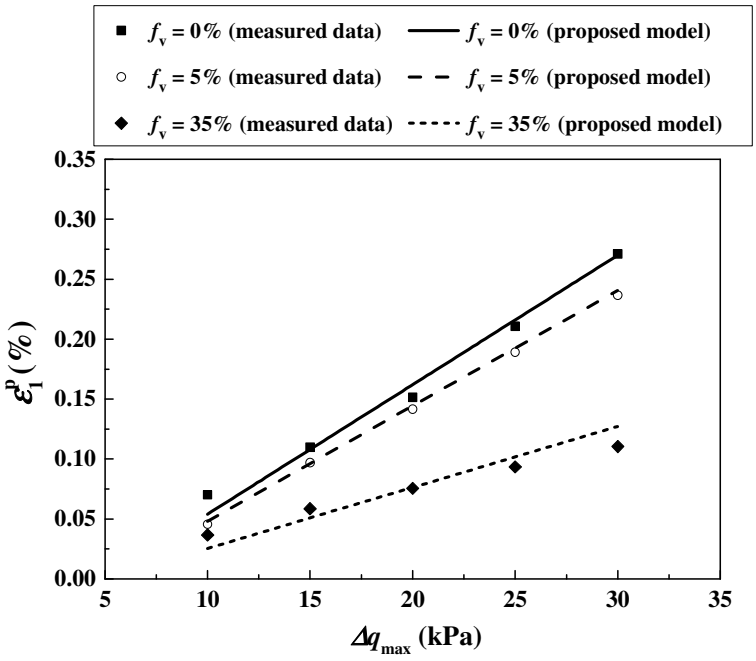

Fig. 6. Linear fitting of end-stage permanent strain ε_1^p with $\Delta q_{\max}$ using expression $t(f_v, \Delta q_{max})$ at f_v = 0%, 5% and 35%

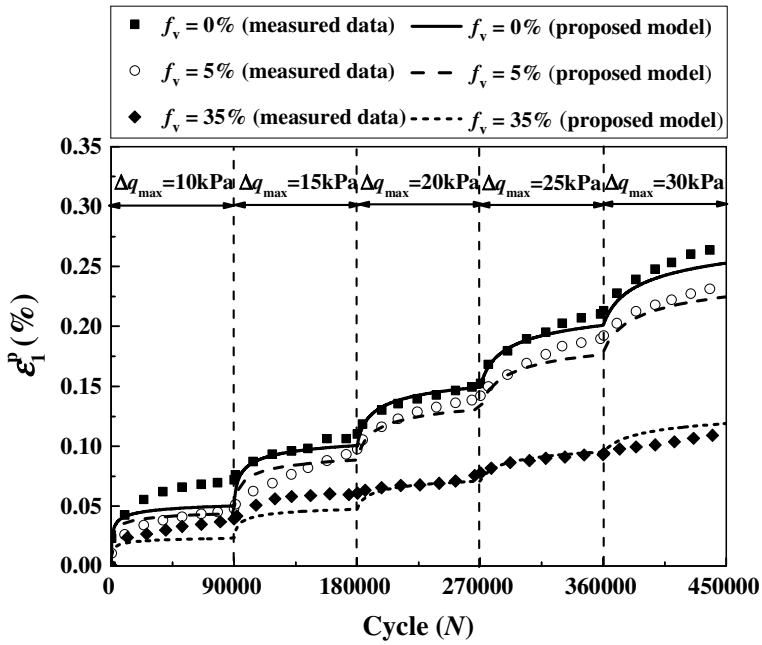

Fig. 7. Determination of parameters by fitting cyclic test results at f_v = 0%, 5% and 35%

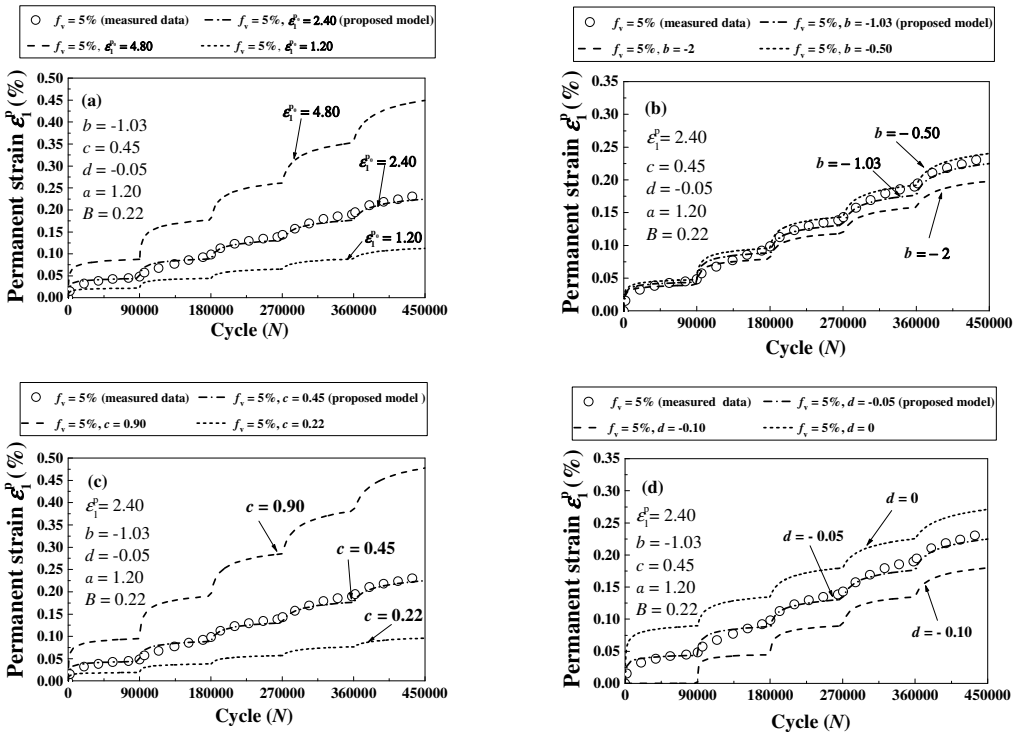

Fig. 8. Effects of parameters $\varepsilon_1^{p_0}$, b, c and d in $t(f_v, \Delta q_{max})$ on permanent strain curve: (a) parameter $\varepsilon_1^{p_0}$; (b) parameter b; (c) parameter c; (d) parameter d

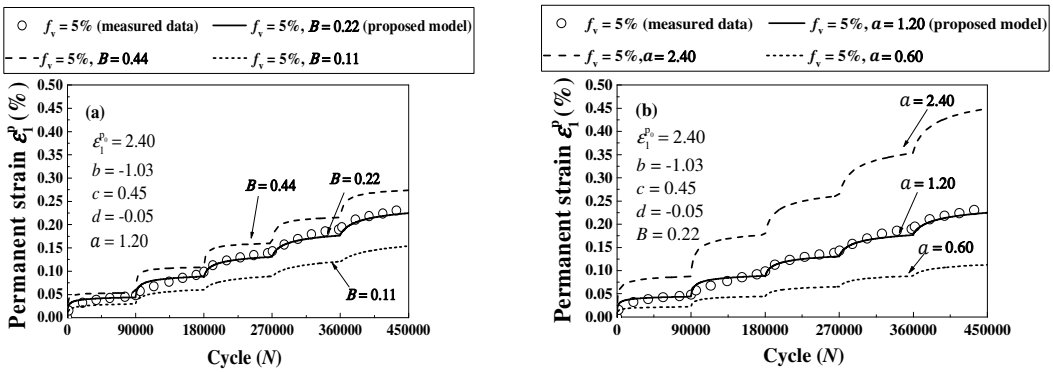

Fig. 9. Effects of parameters a and B in h (N) on the evolution of permanent strain with loading cycles N: (a) parameter B; (b) parameter a

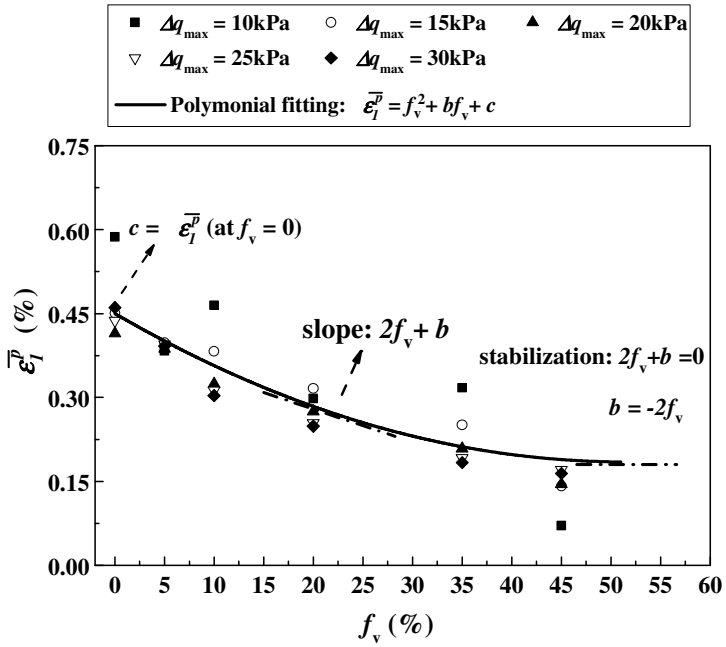

Fig. 10. Variations of end-stage permanent strain $\bar{\varepsilon}_1^p$ with coarse grain content f_v

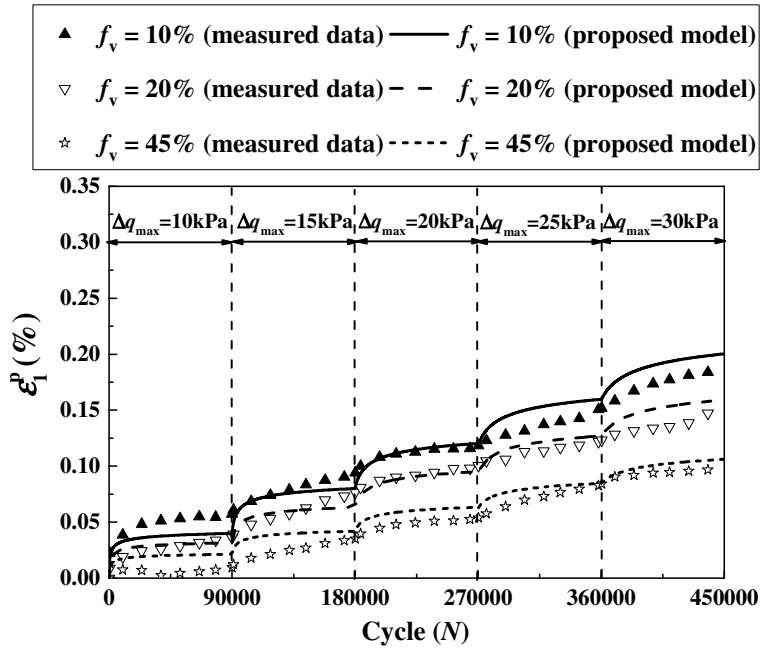

Fig. 11. Simulations of the cyclic test results by the proposed model for f_v = 10%, 20% and 45%